

Precipitation from Supersaturated Aluminate Solutions

II. Role of Temperature

H. A. VAN STRATEN AND P. L. DE BRUYN

Van't Hoff Laboratory, Transitorium 3, Padualaan 8, 3584 CH Utrecht, The Netherlands

Received February 21, 1984; accepted May 15, 1984

The effect of temperature on the precipitation of aluminum hydroxide from dilute potassium aluminate solutions ($C_{\text{Al(OH)}_4^-} = 4 \times 10^{-3} M$) was studied in acid titration and pH-stat experiments. The precipitation sequence is largely dictated by the supersaturation (II) and follows the Ostwald rule of stages: amorphous \rightarrow pseudoboehmite \rightarrow bayerite \rightarrow gibbsite. The precipitation boundaries, $-\log a_{\text{Al(OH)}_4^-}/a_{\text{OH}^-}$, of the amorphous phase (-1.9) and pseudoboehmite (-1.2) evaluated by interpretations of relaxation time curves are temperature insensitive. The interpretation of relaxation curves in the supersaturation region where pure bayerite forms is based on a surface nucleation mechanism and allows estimates of the free energy of formation of the critical nucleus (~ 20 kJ/mole), interfacial tension and two activation energies (-30 kJ/mole, $+95$ kJ/mole). The preferred formation of pseudoboehmite at high pOH is shown to be the result of a lower interfacial energy and the retarding effect it exerts at all temperatures on the competing growth of bayerite crystals. The growth rate of bayerite is shown to be proportional to the available surface and the square of the supersaturation and is characterized by an activation energy of about 60–80 kJ/mole. © 1984 Academic Press, Inc.

INTRODUCTION

In a previous publication (1) we reported on the formation of different aluminum hydroxide phases from supersaturated aluminate solutions at room temperature. Under the experimental conditions investigated, the observed precipitation sequence (amorphous–pseudoboehmite–bayerite) was noted to conform to the so-called Ostwald rule of stages (2). From a detailed analysis of the relaxation behavior of the supersaturated solutions at constant pH, it became apparent that the nucleation and growth of the most stable solid phase (bayerite) was retarded by heterogeneous nucleation of pseudoboehmite. Experiments carried out at different aluminate concentrations and pH values revealed the relaxation behavior to be determined mainly by the degree of supersaturation (II).

In this paper we report on the influence of temperature on the relaxation behavior of supersaturated aluminate solutions with an

initial aluminate concentration (c_{Al}) of $4 \times 10^{-3} M$ and an ionic strength of $0.15 M$ (KNO_3). We are interested in the temperature dependence of the different processes which were shown to be responsible for the relaxation behavior at room temperature and the evaluation of the activation energy from such measurements. Furthermore, as it is generally reported (3–5) that the formation of the most stable solid modification (gibbsite) from aluminate solutions is favored kinetically at higher temperatures, we are also interested in establishing how this phase modifies the already complex precipitation behavior.

EXPERIMENTAL

The precipitation of the solid phase from supersaturated aluminate solutions in the temperature range, 25 to 90°C was studied by the same experimental techniques described in the earlier publication (1). Freshly diluted stock solutions containing 4×10^{-3}

M aluminate, an OH/Al ratio of 6.66 and of total ionic strength $0.15 M$ (KNO_3) were titrated with an $0.25 M$ HNO_3 solution in a reaction vessel (final volume 3 liters) of special design. All chemicals were of reagent grade, freshly twice-distilled water was used and the titration was performed under a nitrogen atmosphere to eliminate CO_2 . The temperature during the titration and pH-stat experiments was controlled by means of a Lauda NB-S15 thermostat. Electrodes (Type Ingold HA 465-35-90 with a double liquid junction) were calibrated before and after each experiment at the measuring temperature with standard Electrofact buffers (pH values 6.98 and 9.18 at $25^\circ C$). In the titration experiments the titrant was added at a constant rate and pH of the solution was followed with a Mettler pH-meter connected to a recorder. In the pH-stat experiments, the amount of acid needed to maintain a constant pH was supplied by an automatic burette and was registered by a recorder. Samples taken from the reaction vessel were pressure-filtered through Millipore paper ($0.65 \mu m$), washed with twice-distilled water and air-dried at the temperature of preparation. The solids were characterized by X-ray, IR, EM, and BET adsorption techniques.

RESULTS

a. Titration Experiments

In our studies at $25^\circ C$ (1) for relatively fast titrations a characteristic pseudoequilibrium curve was obtained when plotting pH or $pH + pAl_T$ (in the case of varying total aluminate concentration, Al_T) against the ratio, OH/Al. In alkaline solutions the temperature dependence of the pH at constant pressure (P) and amount of base (m_{KOH}) may be expressed by the relation

$$\left(\frac{dpH}{dT}\right)_{P, m_{KOH}} = \left(\frac{dpK_w}{dT}\right)_{P, m_{KOH}} - \left(\frac{dpOH}{dT}\right)_{P, m_{KOH}} \quad [1]$$

where K_w is the dissociation constant of water. When the concentration of hydroxyl ions is large compared to that of hydrogen ions, as would be true even for weakly alkaline solutions, Eq. [1] shows that

$$\left(\frac{d(pOH)}{dT}\right)_{P, m_{KOH}} \simeq 0 = \left(\frac{dpK_w}{dT}\right)_{P, m_{KOH}} - \left(\frac{dpH}{dT}\right)_{P, m_{KOH}} \quad [2]$$

There is a negligible temperature dependence of the pOH of a solution at fixed amount of added base, whereas the change in pH under these conditions is determined largely by the temperature coefficient of the water dissociation constant K_w . This analysis suggests that a comparison of titration results at different temperatures should be done preferably by plotting pOH (rather than pH) versus OH/Al. Such a plot is given in Fig. 1 for three different temperatures (25 , 50 , and $60^\circ C$) and the same constant titration speed of $0.024 \text{ mole acid mole}^{-1} \text{ Al min}^{-1}$.

The titration curves may again be divided into two regions. In region A essentially neutralization of excess alkali occurs. We also note that here Eq. [2] is well obeyed. Precipitation takes place in region B. The drop in pOH at 50 and $60^\circ C$ (curves a and b) implies that the rate of solid phase formation exceeds the titration speed. At $25^\circ C$ (curve c), for the same titration speed, a

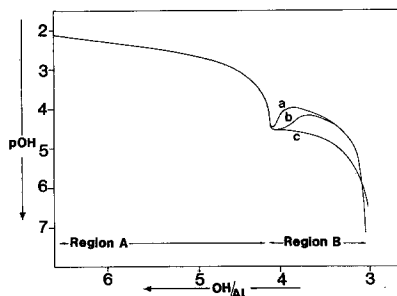


FIG. 1. Titration curves (pOH vs OH/Al) at constant acid addition rate ($0.024 \text{ mole } H^+ / (\text{mole Al min})$). (a) $60^\circ C$; (b) $50^\circ C$; (c) $25^\circ C$. Initial aluminate concentration: $4 \times 10^{-3} M$, ionic strength $0.15 M$.

pseudoequilibrium state is approached. This kinetic behavior is clearly illustrated in Fig. 2 where the effect of different titration rates on the kinetics of precipitation in region B at a temperature of 50°C is presented. Only at the highest acid addition rate (0.18 mole acid mole⁻¹ Al min⁻¹) the characteristic pseudoequilibrium curve (see the titration curve c at 25°C in Fig. 1) is registered. Lowering the titration speed increases the relative rate of solid phase formation and at the lowest rate of acid addition (0.005 mole acid mole⁻¹ Al min⁻¹) even a two-step process (indicated by two dips in the titration curve) becomes evident.

Solid state analysis of the precipitates showed that at high titration rates an amorphous phase is formed (titration curve at 25°C in Fig. 1 and curve a in Fig. 2), whereas on lowering the rate of acid addition or increasing the temperature, increasing amounts of pseudoboehmite precipitate (Fig. 1 and curves b and c in Fig. 2) formed. In the titration experiment (curve d, Fig. 2) small amounts of bayerite were also detected and at the lowest titration speed (curve c, Fig. 2) the increased amount of this crystalline phase is evidenced by the second dip in the curve. Small amounts of gibbsite were also noted in the latter experiment.

In general it may be stated that the occurrence of a pseudoequilibrium titration curve

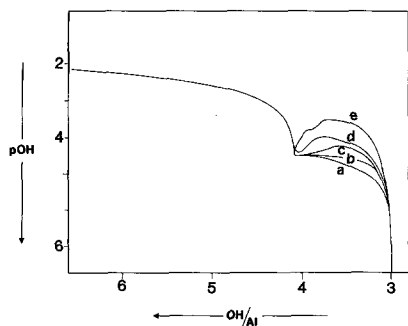


FIG. 2. Titration curves at constant temperature (50°C) for five different addition rates in mole H⁺/(mole Al min). (a) 0.18; (b) 0.091; (c) 0.044; (d) 0.019; (e) 0.005. Initial aluminate concentration: 4×10^{-3} M, ionic strength 0.15 M.

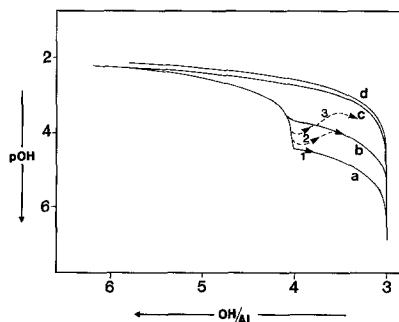
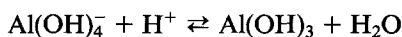


FIG. 3. Theoretical equilibrium titration curves at 50°C for four different phases. Estimated solubility products ($pK = -\log(a_{\text{Al}(\text{OH})_3}/a_{\text{OH}^-})$): (a) Amorphous $pK = -1.9$. (b) Pseudoboehmite $pK = -1.1$. (c) Bayerite $pK = 0.3$. (d) Gibbsite $pK = 0.87$. Three kinetic paths are indicated resembling actual experiments (see Figs. 1 and 2).

is determined kinetically by the titration speed and temperature. For example, at 25°C deviation from the (pseudo) equilibrium formation of an amorphous solid phase was observed by Stol (6) to occur only at titration speeds lower than 0.003 mole acid mole⁻¹ Al min⁻¹. We have shown (1) that the pseudoequilibrium curve for the amorphous solid phase at 25°C may be synthesized by assuming two fast equilibrium reactions



$$K_2 (25^\circ\text{C}) \simeq 8 \times 10^{-13}.$$

Hypothetical equilibrium titration curves for the formation of the other solid modifications can be calculated in an analogous way if the appropriate solubility product is known. In Fig. 3 we present calculated equilibrium titration curves for the different Al(OH)₃ solid phases based on estimated values of the solubility products at 50°C. Note that curve d, the equilibrium curve for the formation of gibbsite, will only be obtained at extremely low titration rates.

From nucleation theory we know that a critical supersaturation is needed for the formation of a significant number of critical nuclei after which growth of the new phase may proceed at a rapid rate. This happening

will be detected in the titration curve as a drop in the pOH value. Once a certain pOH value is exceeded the growth process will be faster than the acid addition. In Fig. 3 we have sketched a few precipitation paths which resemble the experimental titration curves observed by Stol at room temperature (6) and by us at higher temperatures. Path 1 will be followed at high titration rates and will coincide with the calculated curve for the amorphous phase. Apparently this phase forms at relatively low supersaturations as is evidenced by the absence of a dip in the titration curve over a 10-fold change in titration speed (1). Path 2 will be obtained at intermediate titration rates where the drop in pOH corresponds to rapid growth of pseudoboehmite once a certain pOH value is reached. Path 3 will be followed when, in succession, pseudoboehmite and bayerite form (two dips). Although the qualitative interpretation of the experimental titration curves is straightforward as illustrated by Fig. 3, a quantitative determination of solubility products from such curves is hazardous.

b. pH-Stat Experiments

In these experiments our attention was focussed on relaxation experiments at pOH values in region A (Fig. 1) where immediate formation of the amorphous phase could not take place. From experiments conducted at different temperatures and pOH values we are able to distinguish four types of relaxation curve. Representative examples of these types are displayed in Fig. 4, based on experiments performed at 50°C at different pOH values and hence varying initial supersaturations. The experiments were actually performed at a constant pH but because of the water dissociation equilibrium (7) this also implies constant pOH. The ordinate axis in these relaxation curves describes the normalized uptake of acid, $\alpha(t) = \Delta[H^+(t)]/Al_T$ where $\Delta[H^+(t)]$ is the cumulative uptake of acid at time t and Al_T is the total amount of aluminate.

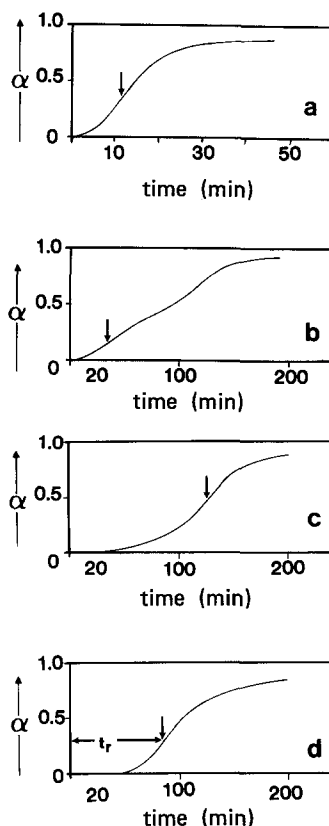


FIG. 4. Types of relaxation curves (α versus t) at 50°C. Arrows locate time at which uptake rate is at its maximum. (a) pOH 4.35, (b) pOH 4.15, (c) pOH = 4.05, (d) pOH = 3.75.

At a high pOH value (high supersaturation) a regular S-shaped relaxation or acid uptake curve is registered (Fig. 4a), it is replaced at a slightly lower pOH (lower supersaturation) by a curve characterized by two inflection points (Fig. 4b), which in turn is succeeded by a typical curve illustrated in Fig. 4c which at the lowest pOH value again becomes S-shaped (Fig. 4d). At supersaturations higher than those characteristic of Fig. 4a rapid formation of an amorphous phase ensues, a situation which we wished to avoid. The same sequence of relaxation curves depicted in Fig. 4 was also found at 75 and 90°C. At 25°C (1) the relaxation curves, types b, c, and d, were also observed but not type a. At this temperature type b curve persisted until

the precipitation boundary for the amorphous phase was reached, then a three-step curve appeared where the fast initial uptake of acid (formation of amorphous phase) is followed by a curve similar to type b in Fig. 4. The four types of relaxation curve (Fig. 4) are closely connected with changes in the nature of the precipitating solid phases. At high supersaturations (Fig. 4a) only pseudoboehmite was observed to form, at somewhat lower supersaturations (Fig. 4b) pseudoboehmite formed initially and in the second stage (beyond the second inflection point) mainly bayerite formed. At low supersaturations (Fig. 4d) almost exclusively bayerite formed except that at higher temperatures (75–90°C) noticeable amounts of gibbsite were also seen. The formation of gibbsite was, however, never indicated by an inflection point in the relaxation curve, in sharp contrast to the appearance of bayerite after pseudoboehmite (Fig. 4b).

In Fig. 5 we give a schematic presentation of the type of solid phases present in the end product of the relaxation experiments ($\alpha(\text{end}) \approx 0.8 \pm 0.1$ for most experiments) as a function of pOH and temperature. A rough estimate of the relative amounts of the various solid modifications is also included in Fig. 5. The information displayed is based on relax-

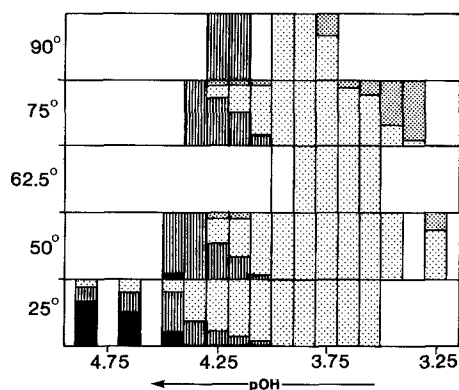


FIG. 5. Histogram of the solid phases formed as a function of temperature and pOH. The lower parts of the diagrams represent in general the first phase which is formed. ■ Amorphous. ▨ Pseudoboehmite. ▩ Bayerite. ▤ Gibbsite

ation curves and X-ray and IR analyses. The phase which is indicated in the lower part of the composition block (rectangle) is in most cases the first phase to form at that pOH and temperature. We note that the sequence in which the different phases precipitate is largely determined by the pOH value. Especially at 75 and 90°C, large amounts of gibbsite are seen to form at low pOH values. Remarkable is the occurrence at 50°C of small amounts of gibbsite at high pOH values where also pseudoboehmite forms; it could not be detected at low pOH values where bayerite predominantly forms. We also note that bayerite which is present in overwhelming amounts at 25°C over a wide pOH range is displaced kinetically by pseudoboehmite at high pOH values and by gibbsite at low pOH values, when the temperature is increased. It should be realized, however, that this kinetic precipitation diagram is representative for relatively fast relaxation experiments (duration 1–10 hr) and that aging of the end products in the mother liquor could involve further phase transformations. Although this effect was not investigated in detail an interesting result was obtained on aging pseudoboehmite samples at the ambient temperature and pOH 4.35. At 50°C a substantial amount of this solid modification was observed to transform into bayerite over a period of a few weeks (24 hr \sim 15%, 3 weeks \sim 80% transformation), however, at 75°C pseudoboehmite was still present in large amounts after an aging period of 4 weeks. This kinetic phenomenon may be correlated with the results of Chang (8) who concluded from an analysis of the thermodynamic data that the transition temperature between gibbsite and boehmite is $60 \pm 3^\circ\text{C}$ with the former phase more stable below this temperature. Above this temperature it is then more likely that pseudoboehmite transform directly into boehmite.

A characteristic difference between pseudoboehmite and bayerite is the much higher specific surface of the former compared to the latter. In Fig. 6 the BET specific surfaces

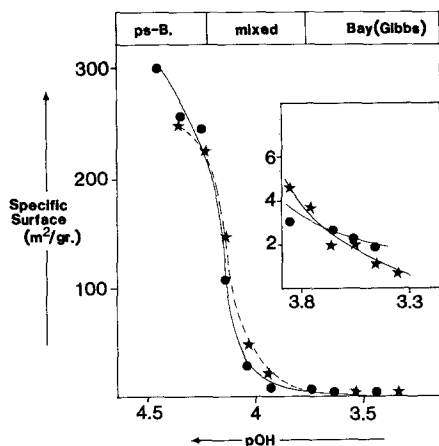


FIG. 6. Specific surface area (m^2/g) as a function of pOH at 50 and at 75°C . The inserted figure is an enlargement of the values between pOH 3.5 and pOH 4.3; (●) 50°C ; (×) 75°C .

of the end product of relaxation experiments is plotted against pOH at two temperatures (50 and 75°C). We note that pseudoboehmite has a specific surface area of about $250 \text{ m}^2/\text{g}$ whereas the specific surface area of bayerite (or gibbsite) is approximately lower by 2 decades. The sharp drop in the BET surface area around a pOH value of 4.1 is connected with the transition region between pseudoboehmite and bayerite. A similar conclusion was drawn from measurements at 25°C (1).

In Fig. 7 some typical electronmicrographs are given of the final products obtained in the pseudoboehmite-region and in the bayerite-region. Although at first glance the bayerite particles appear to be somewhat irregular in shape, they clearly show a tendency to grow with a conical form. A similar observation was made by Violante and Violante (23). Figure 7c illustrates practically all the particles to exhibit a hill-and-valley structure that is indicative of growth initiated by the formation of two-dimensional nuclei. The irregular nature of the growth ends suggests that nucleation and outgrowth of these nuclei is a continuous and simultaneous process.

DISCUSSION

Titration and pH-stat experiments revealed the possible formation of four distinct solid

phases during precipitation of supersaturated aluminate solutions. It was possible to deduce the precipitation sequence

amorphous \rightarrow pseudoboehmite \rightarrow

bayerite \rightarrow gibbsite

from experiments in which the aluminate solution was apparently supersaturated with respect to all of these solid modifications. This sequence is seen to be in accord with the Ostwald rule of stages which predicts that the thermodynamically least-stable phase should form first. Of fundamental interest to the understanding of this complex precipitation system would be an evaluation of the nucleation and growth characteristics of each of the four phases. To accomplish this objective conditions must be established under which the formation of a given solid phase may be followed kinetically without interference by other precipitating phases.

The titration experiments indicated that an amorphous phase is formed immediately once a certain value of the supersaturation ($\text{pAl} - \text{pOH} \leq -1.9$) is reached and the titration speed lies above a limiting value. It is, however, clear that the kinetics of formation of this phase would require measurement of times in the (milli-) second range. This requirement could not be met by our experimental approach. The titration experiments at relatively low titration rates and the pH-stat experiments did enable us to study the kinetics of precipitation of the other three solid phases. In addition we were able to arrange the experimental conditions so that it was possible to observe the separate formation of bayerite and pseudoboehmite. It was not possible to establish precipitation conditions where gibbsite may be said to form without interference of bayerite. This failure would seem to imply that the kinetics of the formation of these two crystalline phases is not significantly different.

Relaxation Behavior of the Precipitating System

Quantitative information about the nucleation kinetics may be extracted from the

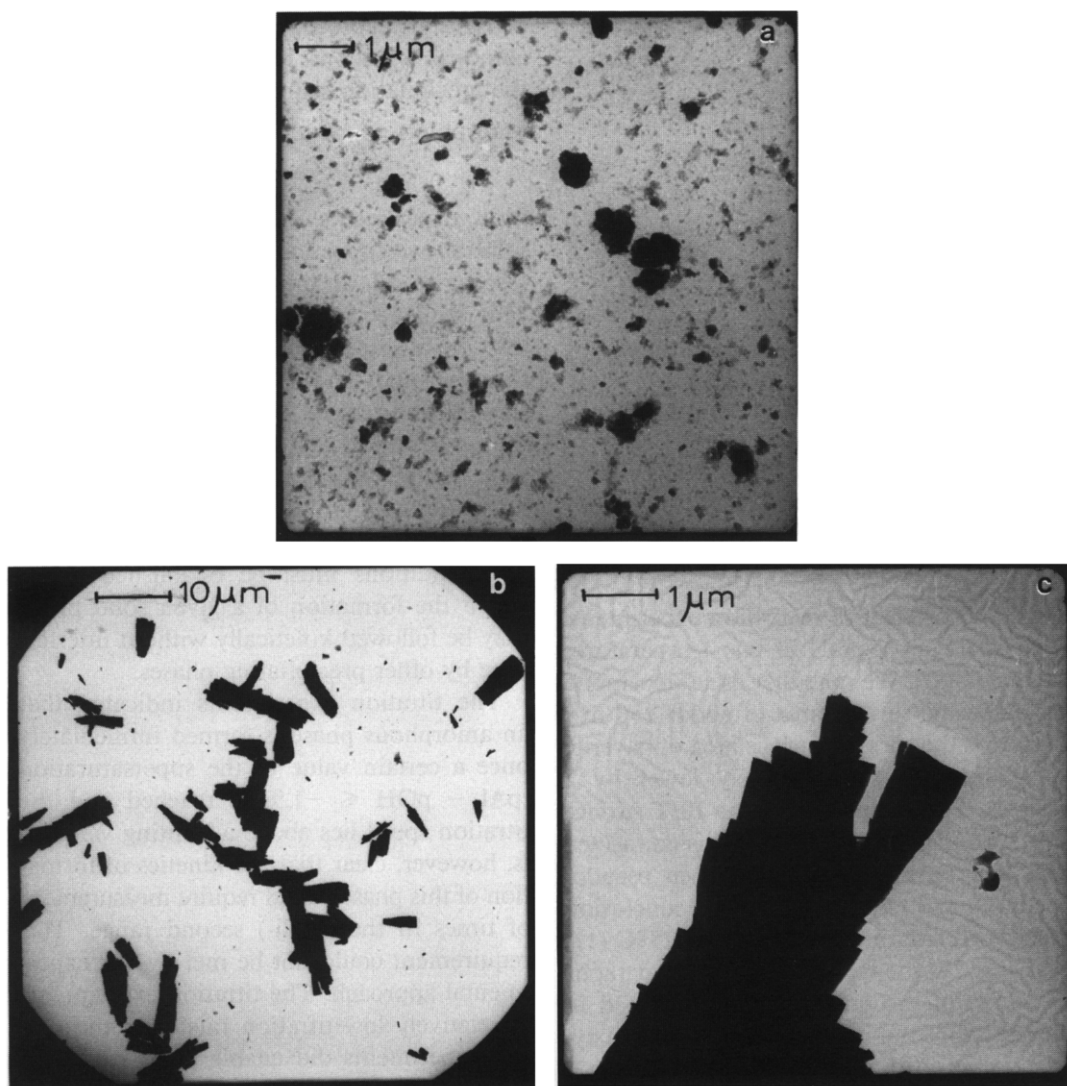


FIG. 7. Electronmicrographs of samples obtained in experiments where mainly pseudoboehmite (a) and bayerite (b) and (c) are formed. (c) the typical hill-and-valley structures observed with bayerite particles. (a) Pseudoboehmite, 50°C, pOH 4.35; (b/c) bayerite, 50°C, pOH 3.55.

relaxation (pH-stat) experiments by introducing a relaxation time, t_r (1). This parameter is defined as the time at which the uptake-rate of acid (da/dt) reaches a maximum (see Fig. 4).

Figure 8 gives a plot of the relaxation time (t_r) as a function of pOH at three different temperatures. At 25°C, the relaxation times at all pOH values refer to the times for maximum rate of uptake of acid in the

formation of bayerite. Only the right-hand branch of this curve (pOH \leq 3.85) describes the relaxations in which pure bayerite forms (1). At 50 and 75°C it was possible to separate in time the formation of bayerite and pseudoboehmite. At pOH values higher than that indicated by arrow A (see Fig. 8) the relaxation times refer to the formation of pure pseudoboehmite and at pOH values lower than that indicated by arrow B the relaxation

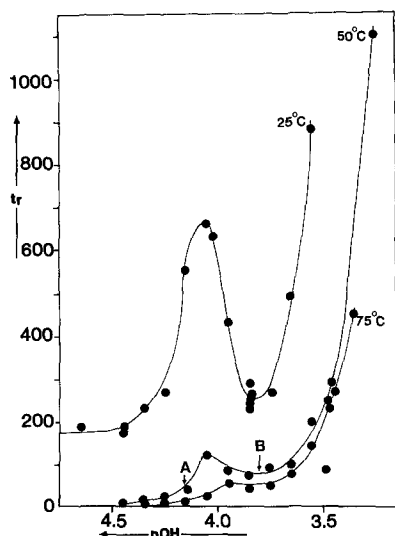


FIG. 8. Relaxation times (t_r) as a function of pOH at 25, 50, and 75°C. At 25°C the t_r -values in the left-hand branch refer to bayerite in the presence of (considerable) amounts of pseudoboehmite.

times describe the formation of pure bayerite. The relaxation times which determine the behavior of the curves in the region between arrows A and B refer to the formation of bayerite under conditions where both phases are known to be present. The same general shape of the relaxation curves is seen to characterize the precipitation at all three temperatures except that the height of the maximum in the curve is significantly reduced at 50 and 75°C. We conclude from Fig. 8 that the same type of kinetic processes are operable at the different experimental temperatures. At low pOH values a regular decrease in t_r is measured for the bayerite (or gibbsite) phase. In the region where small amounts of pseudoboehmite form the relaxation time increases with increasing pOH and at high pOH values where pseudoboehmite is a major (or sole) constituent a smooth decrease in t_r is again measured. We have argued previously (1) that the minimum in the curve at higher pOH values (at 25°C) is due to the fact that heterogeneous formation of small amounts of pseudoboehmite on bayerite particles retards further growth of

bayerite. This explanation remains valid at higher temperatures except that the retardation effect is less pronounced. The observed maxima at these higher temperatures are clearly due to the increased rate of nucleation of pseudoboehmite with increasing pOH as expressed by the drop in t_r . At 25°C this decrease in relaxation time at high pOH values is also observed but under these conditions the formation of bayerite and of pseudoboehmite are not always clearly separated in time. The formation of both phases must be accelerated by increasing pOH in this pOH range, although the formation of one phase may be relatively enhanced compared to the other.

The pOH of a supersaturated solution is not a satisfactory measure of the degree of supersaturation when one wishes to compare precipitations at different temperatures. The most general expression for the supersaturation Π_i of the aluminate solution with respect to solid phase i is

$$p\Pi_i = pAl - pOH - pK_{sp,i}(T) \quad [3]$$

where the solubility product $K_{sp,i}$ is defined by

$$K_{sp,i} = \frac{a_{Al(OH)_4^-}}{a_{OH^-}} \quad [4]$$

and $pAl = -\log a_{Al(OH)_4^-}$.

As the solubility product is a function of temperature we note from Eq. [3] that only at a fixed temperature will changes in $p\Pi_i$ be independent of the nature of the solid phase which forms, and can pOH be used as a useful relative measure of the supersaturation. Unfortunately, except for gibbsite, the temperature dependent solubility products of the various solid phases are not accurately known. In Fig. 9 we have plotted $\log t_r$ versus $\log \times \Pi_{gibbsite}$. The supersaturations with respect to gibbsite were calculated from published data by different investigators (9–12). The results of some experiments at 62.5 and 90°C are also included in this figure.

The displacement of the relaxation curves at different temperatures is due to the strong increase in the solubility of gibbsite with

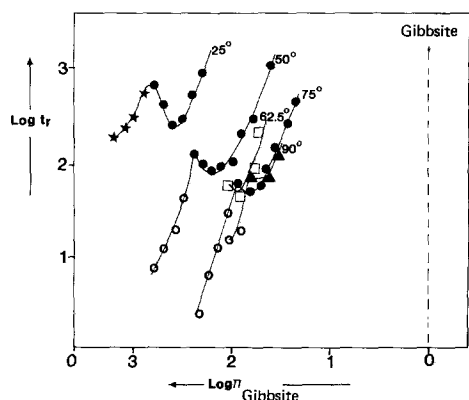


FIG. 9. $\log t_r$ (min) versus the supersaturation ($\log \times \Pi_{\text{gibbsite}}$) with respect to gibbsite at 25, 50, 62.5, 75, and 90°C. (●) bayerite at 25, 50, and 75°C. (□) bayerite at 62.5°C, (▲) bayerite at 90°C, (×) bayerite at 25°C in presence of substantial amounts of pseudoboehmite, (○) pseudoboehmite at 50, 75, and 90°C.

increasing temperature. The two branches of the relaxation curves corresponding to pure bayerite and pure pseudoboehmite formation are clearly defined in this logarithmic plot. We have previously shown (see, for example, Fig. 5) that replacement of bayerite by gibbsite at higher temperatures in the precipitation sequence occurs without any detectable change in shape of the relaxation curve (α vs t). This observation considered together with the similarity in the structure of these two crystalline modifications suggest that the temperature dependence of the solubility of bayerite is of the same order of magnitude as that of gibbsite. Hence the same shift in the relaxation curves depicted in Fig. 9 would occur if instead of $\log \Pi_{\text{gibbsite}}$, $\log \Pi_{\text{bayerite}}$ were to be plotted against $\log t_r$. We may then conclude that at a fixed value of supersaturation the relaxation times for bayerite will decrease with increasing temperature.

We have seen that the lowering of the relaxation time of bayerite with increasing supersaturation (or pOH) at a fixed temperature is arrested by the heterogeneous nucleation of pseudoboehmite. If it is assumed that the composition of the solution at which this retardation effect becomes just detectable, corresponds to the precipitation boundary ($p\Pi = 0$) for pseudoboehmite, the tempera-

ture dependence of the solubility product of pseudoboehmite may be estimated. It appears then that the solubility product of pseudoboehmite is relatively insensitive to changes in temperature over the range of temperatures employed in this study. We estimate $-1.2 > pK_{\text{sp}} > -1.3$ although this estimate may be somewhat on the low side because even for heterogeneous nucleation a slight supersaturation is needed. Based on the above estimate the supersaturation with respect to pseudoboehmite is found to be related to the pOH by the expression, $\text{pOH} \approx 3.7 - p\Pi_{\text{pseudoboehmite}}$. The graphs in Fig. 8 may thus also be interpreted as depicting the change in t_r with a change in the supersaturation with respect to pseudoboehmite.

Nucleation in Single (Solid) Phase Domains

Under conditions where only one solid phase is precipitating, the experimental relaxation time curves may be analyzed by application of classical nucleation theory (13). According to this theory we may write

$$t_r = \tau'_0(T) \exp(\Delta G_c/kT) \\ = \tau_0 \exp[(E_{\text{act}}^{(1)} + \Delta G_c)/kT] \quad [5]$$

where τ_0 is some reciprocal frequency factor and independent of temperature, $E_{\text{act}}^{(1)}$ is an apparent activation energy for the various transport processes involved in the nucleation step, and ΔG_c is the free energy of formation of a critical nucleus.

In the case of three-dimensional (3D) nucleation we write

$$\Delta G_c(3D) = \frac{Av^2\sigma^3}{(kT)^2(\ln \Pi)^2} \quad [6]$$

and if a two-dimensional nucleation step is rate-determining

$$\Delta G_c(2D) = \frac{Bv^{4/3}\sigma^2}{kT \ln \Pi} \quad [7]$$

In these expressions σ is the interfacial tension, v the mean ionic volume of the solid phase, k the Boltzmann constant, and A and B are constants determined by the geometrical

shape of the critical nucleus. In writing Eq. [7] we have assumed a linear relation between the edge free energy (or line tension) ρ and the interfacial tension,

$$\sigma = \rho v^{-1/3}. \quad [8]$$

The relatively fast formation of pseudo-boehmite and especially the high specific surface area ($\sim 250 \text{ m}^2/\text{g}$) of this phase serve, in our view, as indications that three-dimensional homogeneous nucleation is rate-determining for the overall precipitation process. On the other hand, the slow (order of hours) formation of the crystalline phase bayerite, the low specific surface (~ 1 to $5 \text{ m}^2/\text{g}$), and the hill-and-valley structure of the growing particles as seen under the electronmicroscope (Fig. 7) suggest that a two-dimensional (surface) nucleation step is rate-determining for the formation of bayerite.

An analysis of the experimental results on the basis of the above discussion is presented in Fig. 10 where we give a plot of $\ln t_r$ versus $(\ln II)^{-2}$ for pseudoboehmite and of $\ln t_r$ versus $(\ln II)^{-1}$ for bayerite, both at 50°C . A straight-line behavior is noted in both plots over a supersaturation range where no interference by the other phase is known to occur. The two arrows in the figure locate the supersaturation values at which the second phase (pseudoboehmite or bayerite) makes

its appearance. From these plots one may then calculate τ_0 , ΔG_c , and σ . We believe that attempts to derive absolute values of the interfacial tension are not only unwarranted but would be misleading. However, when different solids are compared or one solid under different conditions, for example, at different temperatures, changes in σ , or some relative measure of σ , may provide useful indications of certain trends.

As can be seen from Eqs. [6] and [7] in order to evaluate σ from plots such as shown in Fig. 10 the molecular volume v , the shape factor, and some relation between σ and ρ must be known. These parameters are not accurately known, certainly not for particles of the size of a critical nucleus. We avoid this difficulty by defining an operational "interfacial tension,"

$$\begin{aligned} \sigma^* &= (k/\sqrt{B})T \cdot \beta^{1/2} \quad \text{for 2D nucleation} \\ &= (k/A^{1/3})T \cdot \delta^{1/3} \quad \text{for 3D nucleation} \quad [9] \end{aligned}$$

where β and δ are the respective slopes of the plots of $\ln t_r$ vs $(\ln II)^{-1}$ and $\ln t_r$ vs $(\ln II)^{-2}$ (see Fig. 10). From Eq. [9] we then deduce that

$$\sigma^* = \sigma \cdot v^{2/3}. \quad [10]$$

In order to derive values for σ^* and $\ln \times \tau'_0(T)$ the solubility products (K_{sp}) of the various phases must be known. A value of 0.7 has been estimated at 25°C (9, 12) for $pK_{sp}(\text{bay}) = -\log(a_{\text{Al}(\text{OH})_4}/a_{\text{OH}^-})$. To evaluate $pK_{sp}(\text{bay})$ at higher temperatures we assume this phase to have the same temperature dependence as gibbsite (9–11). This means that ΔH° for the reaction $\text{Al}(\text{OH})_4^-(\text{aq}) \rightarrow \text{Al}(\text{OH})_3(\text{s}) + \text{OH}^-(\text{aq})$ must be approximately the same for bayerite and gibbsite—a reasonable assumption. For pseudoboehmite we choose $pK_{sp} = -1.1$ a value that is slightly higher than that estimated from an analysis of the data in Fig. 9.

The calculated values of $\ln \tau'_0(T)$, σ^* and some typical values of ΔG_c at four different temperatures are listed in Table I. It can be seen that both σ^* and ΔG_c decrease with temperature and are higher than the pseudoboehmite. If we were to assume that two-

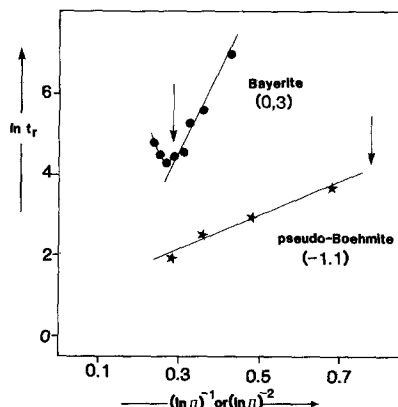


FIG. 10. Plots of $\ln t_r$ versus $1/\ln II$ for bayerite at 50°C and versus $1/(\ln II)^2$ for pseudoboehmite at 50°C . Values between parenthesis refer to the chosen solubility product ($\text{pH} = -\log a_{\text{Al}(\text{OH})_4}/a_{\text{OH}^-}$) for the solid phase.

TABLE I

Parameters Describing Kinetics of Nucleation and Growth in Aluminate Systems

Temp. (°C)	Phase	pK_{sp}	$\ln \tau'_0(T)$	β or δ (Eq. [9])	σ^* (kJ mole ⁻¹)	ΔG_c (kJ mole ⁻¹)	p (H ⁺)	m (Al)	n (H ⁺)
25 ^a	Bay	0.7	-2.3 ± 1.3	36 ± 6	7.4 ± 0.6	21.2 ± 3.5	2.2 ± 0.1	2.0 ± 0.1	1.4 ± 0.3
25	Bay	0.7						1.9 ± 0.2	1.7 ± 0.4
50	Bay	0.3	-1 ± 0.4	19 ± 1	5.9 ± 0.1	15.5 ± 0.8	2.4 ± 0.3	2.05 ± 0.05	2.25 ± 0.2
62.5	Bay	0.1	-3.3 ± 2.9	22 ± 8	6.5 ± 1.1	21.7 ± 8		2.0 ± 0.1	
75	Bay	-0.05	-0.2 ± 0.3	11.5 ± 0.3	4.9 ± 0.1	13.4 ± 0.4	2.4 ± 0.1	1.9 ± 0.1	2.4 ± 0.2
50	ps-B	-1.1	$+0.9 \pm 0.2$	4.2 ± 0.3	1.35 ± 0.05	4.0 ± 0.3	2.6 ± 0.2	$0.8^b \pm 0.1$	2 ± 0.2
75	ps-B	-1.1	-0.8 ± 0.5	5.1 ± 0.9	1.6 ± 0.1	5.2 ± 0.9	3.5 ± 0.2	$1^b \pm 0.1$	3.4 ± 0.2

Note. ΔG_c is calculated at pOH 3.65 for bayerite and at pOH 4.35 for pseudoboehmite; for the calculation of σ^* we assumed the shape factors to be, respectively, $B = 4$ (square) and $A = 32$ (cubic). $E_{act}^{(1)} = -30 \pm 10$ kJ mole⁻¹; $E_{act}^{(2)} = 95 \pm 10$ kJ mole⁻¹; $E_{act}^{(g)} = 60-80$ kJ mole⁻¹.

^a $pAl_T = 1.8$ otherwise $pAl_T = 2.4$.

^b Order in $(c_{Al} - c_{Al,e})$.

dimensional nucleation is also rate-determining for the formation of pseudoboehmite the calculated σ^* values for this phase would be approximately higher by a factor two but still less than those for bayerite. The determination of $\ln \tau'_0(T)$ is less accurate because of the long extrapolation required (see Fig. 10). In principle we can calculate the activation energy $E_{act}^{(1)}$ (see Eq. [5]) from Arrhenius plots of $\ln \tau'_0$ vs $1/T$. On taking into account the inaccuracies in evaluating $\ln \tau'_0$ we find for bayerite formation an activation energy of -30 ± 10 kJ/mole.

It should be realized that absolute values of σ^* , $\ln \tau'_0(T)$ and $E_{act}^{(1)}$ will depend on the chosen values of the solubility product. Calculations show, however, that on allowing for an uncertainty in the pK_{sp} values at 25°C of as high as ± 0.4 units, would not alter the indicated trends (Table I) in σ^* and the low value of the activation energy.

The negative $E_{act}^{(1)}$ needs further comment. The inaccuracy of the method used for evaluating the activation energy from relaxation times must be considered in any interpretation of the observed negative value. We note, however, that $E_{act}^{(1)}$ has been defined as an effective activation energy for a combination of elementary steps. A negative value may therefore indicate that certain steps in the nucleation process proceed faster at lower

temperatures. It has been argued that extensive hydrogen bonding exists in aluminate solutions at low temperatures (14, 15). The observed breakdown of structure at increasing temperature is suggested to be complete at 75°C (16). Misra and White (17) suggested that hydrogen bonding promotes nucleation at low temperatures and to be ineffective as a promotor above 75°C. This role of hydrogen bonding may be offered as a possible (qualitative) explanation of the negative value of $E_{act}^{(1)}$.

As mentioned earlier the determination of absolute values of interfacial tension from relaxation studies is not reliable. In conclusion we nevertheless wish to quote an order of magnitude estimate of the interfacial tension (σ) for bayerite and pseudoboehmite at 50°C. For bayerite this estimate, based on a square nucleus, a density of 2.5 g/cm³ and a pK_{sp} of 0.7 ± 0.3 , is found to equal 67 ± 20 mN/m. For pseudoboehmite a value of about 25 mN/m is estimated. Considering the various assumptions and inaccuracies involved in making these order of magnitude estimates the results are not unreasonable.

Activation Energies in the Nucleation of Pure Bayerite

We note with reference to Fig. 9 that the experimental results in the supersaturation

region where essentially pure single phases are being formed, may also be approximated by the empirical relation¹

$$t_r = \Phi(T)\Pi^{-p}. \quad [11]$$

The value of the exponent p at different temperatures is obtained from the slope of the curves at Fig. 9 and is listed in Table I. We may also define an activation energy $E_{\text{act}}^{(2)}$ which may be obtained from the temperature dependence of Φ ,

$$\frac{E_{\text{act}}^{(2)}}{R} \equiv \frac{d \ln \Phi(T)}{d(1/T)}. \quad [12]$$

A value of 95 ± 10 kJ/mole is calculated for $E_{\text{act}}^{(2)}$ in the temperature range, $25 \leq T \leq 75^\circ\text{C}$, from an analysis of the plots in Fig. 9. This calculated value is positive and much larger than that derived for $E_{\text{act}}^{(1)}$ (-30 ± 10 kJ/mole).

The relation between these two activation energies may be derived in the following manner. Assuming the validity of the classical nucleation expression, Eq. [5], the following two conditions must be satisfied in the middle of the Π -interval where the approximation, Eq. [11], is valid:

$$t_r (\text{Eq. [5]}) = t_r (\text{Eq. [11]}) \quad [13]$$

$$\frac{d \ln t_r}{d \ln \Pi} (\text{Eq. [5]}) = \frac{d \ln t_r (\text{Eq. [11]})}{d \ln \Pi} = -p. \quad [14]$$

On making use of these conditions and Eq. [7], it is readily shown that

$$\ln \Phi(T) = \ln \tau_0 + \frac{E_{\text{act}}^{(1)}}{kT} + \frac{2\Delta G_{c,M}}{kT} \quad [15]$$

and

$$E_{\text{act}}^{(2)} = E_{\text{act}}^{(1)} + 2\Delta G_{c,M} + \frac{2}{T} \frac{d(\Delta G_{c,M})}{d(1/T)} \quad [16]$$

where the subscript M indicates that $\Delta G_c(T)$ is evaluated at the middle of the appropriate

Π -interval. From the values of ΔG_c listed in Table I and the estimated value of $E_{\text{act}}^{(1)}$ (-30 kJ/mole) we note that the last term on the right-hand side of Eq. [16] makes by far the greatest contribution to the apparent activation energy $E_{\text{act}}^{(2)}$ ($=95$ kJ/mole).

An alternative formulation of Eq. [16] may be derived. According to classical two-dimensional nucleation theory

$$n_c = \frac{\Delta G_c}{kT \ln \Pi} \quad [17]$$

in which n_c is formally the size of the critical nucleus. In view of Eq. [14] this expression also determines the exponent p (see Eq. [11]). On introducing Eq. [17] in Eq. [15] we obtain the desired alternative expression for $E_{\text{act}}^{(2)}$

$$\begin{aligned} \frac{E_{\text{act}}^{(2)}}{R} = & \frac{E_{\text{act}}^{(1)}}{R} + 2p \left(\frac{d \ln \Pi}{d(1/T)} \right)_M \\ & + 2 \ln \Pi \left(\frac{dp}{d(1/T)} \right)_M. \end{aligned} \quad [18]$$

In the experiments the initial aluminate concentration was the same at all temperatures, from Fig. 8 we note that the middle of the Π -interval lies at approximately the same pOH value, and from Table I we observe small changes in p with temperature. Equation [18], may therefore be written in a simplified form

$$\begin{aligned} E_{\text{act}}^{(2)} \approx & E_{\text{act}}^{(1)} - 2pR \left(\frac{d \ln K_{sp}}{d(1/T)} \right) \\ = & E_{\text{act}}^{(1)} + 2p\Delta H^\circ. \end{aligned} \quad [19]$$

With $\Delta H^\circ \approx +30$ kJ/mole (11) and $2 < p < 2.5$ we see that the apparent activation energy $E_{\text{act}}^{(2)}$ is largely determined by the standard enthalpy of the precipitation reaction.

Nucleation of Pseudoboehmite

The observation that at high temperatures pure pseudoboehmite may be grown under conditions (low pOH) where the supersaturation with respect to bayerite is expected to

¹ Nielsen (18) proposed a similar expression for the (homogeneous) nucleation rate ($\sim t_r^{-1}$) over a limited supersaturation region.

be higher than that with respect to pseudobohmite, needs further comment. This experimental fact is, of course, in agreement with the thermodynamic interpretation of the Ostwald rule of stages, however, in view of the available kinetic information, this explanation is too simplistic and in fact unsatisfactory. With reference to Fig. 8 the left-hand branch (decreasing t_r with increasing pOH) of the relaxation curve at 50°C may be assumed to relate to the nucleation rate (inverse of t_r) dependence of pseudobohmite on supersaturation (pOH). The absence of detectable amounts of bayerite in the precipitate may then be cited as evidence that under these conditions the rate of nucleation of bayerite must be much smaller than that of pseudobohmite, and that the kinetic interpretation of the rule of stages is applicable. These conclusions may now be validated by extrapolating the right-hand branch of the relaxation curve which describes the nucleation-rate dependence of pure bayerite (1) into the pseudobohmite-formation field. This extrapolation may be done with the aid of Fig. 10. By following this procedure we estimate that the relaxation times of pure bayerite in the pOH range in which pseudobohmite forms are approximately equal to or slightly higher than the experimental t_r values. The uncertainty in the exact value of the solubility product of bayerite has been allowed for in making this estimate. We must therefore conclude that since the nucleation rate of pure bayerite under these conditions (high pOH) is not much different from that of pure pseudobohmite, the formation of bayerite is effectively blocked (or retarded) by the presence of pseudobohmite. This conclusion is not surprising as we have previously seen that the relaxation behavior of the system in the region where mixed precipitates are present, must be due to retardation of bayerite growth by the presence of small amounts of pseudobohmite. Our analysis of the left-hand branch of the relaxation time curve may then be summarized by writing

$$J_{\text{exp}} \approx J_{\text{psboehm}}^0 \gg \theta J_{\text{bay}}^0$$

where J_i^0 is the nucleation rate of pure phase i and θ is a blocking factor which may vary between 0 and 1 and which is approximately zero in this case. This extrapolation when applied at 75°C shows that at the highest pOH-values the relaxation time is about 3 times smaller than for bayerite. At 75°C it is therefore not necessary to introduce a blocking factor.

We noted earlier in the discussion of Fig. 5 that gibbsite is able to form at high pOH values under circumstances where pseudobohmite developed first. This precipitation sequence may be accounted for by assuming that the pseudobohmite with its high specific surface provides template material onto which other phases may be formed heterogeneously. Formation of gibbsite and not bayerite, becomes possible if the initial precipitation of pseudobohmite causes a substantial lowering of the supersaturation to reach a value where heterogeneous formation of the former phase is favored.

Growth Rates of Solid Phases

As a starting expression for the phenomenological description of the rate of growth, $\dot{R} = da/dt$, of a solid from a supersaturated solution we may write

$$\dot{R} = k(T) \cdot A \cdot f(\Pi) \quad [20]$$

where $k(T)$ is an overall (heterogeneous) reaction rate constant, A is the available surface area, and $f(\Pi)$ is some function of the supersaturation Π . If we approximate the function $f(\Pi)$ by a power function then

$$\dot{R} = k'(T) \cdot A \cdot \Pi^m. \quad [21]$$

This approximation may be justified on the basis of a detailed analysis of our experimental growth curves but also on the theoretical grounds. It has been shown that over limited supersaturation ranges fundamental expressions of the growth rate based on various physical models, agree with a power function dependence on supersaturation. Spiral growth models (19) describing crystal growth at very low supersaturations predict a first order or

second order dependence on the supersaturation. Surface nucleation growth models (20) can give rise to high powers of m , especially at low Π and large interfacial tension. At high supersaturations where the growth rate may be diffusion-controlled m equals unity.

The temperature dependence of the reaction rate constant in Eq. [21] may be expressed by the Arrhenius relation

$$k'(T) = k_0 \exp(-E_{\text{act}}^{(g)}/RT) \quad [22]$$

where $E_{\text{act}}^{(g)}$ is an overall activation energy for growth and includes the contribution of the various elementary steps such as volume diffusion, diffusion through a surface layer, adsorption and dehydration of the growth unit in a kink site.

The available surface for growth may be approximated by the relation

$$A(t) = q\alpha(t)^{2/3} \quad [23]$$

with q a proportionality factor. This expression will hold if, once growth has started, no new nuclei are generated and the shape of the particles does not change during growth. In the ideal case that N spherical nuclei are present initially ($t = 0$),

$$q = \left(\frac{3Al_T M_{\text{Al}} \sqrt{4\pi}}{\rho_{\text{Al}}} \right)^{2/3} \cdot N^{1/3} \quad [24]$$

where Al_T is the total amount of aluminate in the system, and M_{Al} and ρ_{Al} , respectively, the molecular weight, and density of the solid phase, aluminum hydroxide.

On substituting Eqs. [22] and [23] into Eq. [21] and introducing the definition of the degree of supersaturation (Eq. [3]), we find the expression for the growth rate

$$\begin{aligned} \frac{d\alpha(t)}{dt} &= k_0 \exp(-E_{\text{act}}^{(g)}/RT) \cdot q\alpha^{2/3}(t) \\ &\quad \times \frac{[\text{H}^+]^n [1 - \alpha(t)]^m}{K_{\text{sp}}^m} \\ &= k_1 \alpha^{2/3}(t) [1 - \alpha(t)]^m \end{aligned} \quad [25]$$

where

$$\left. \begin{aligned} k_1 &= k_0 \exp(-E_{\text{act}}^{(g)}/RT) q [\text{H}^+]^n K_{\text{sp}}^{-m} \\ &= k_2 [\text{H}^+]^n \end{aligned} \right\} \quad [26]$$

and K_{sp} is the solubility product of the growing phase. The exponents m and n in Eqs. [25] and [26] may not be equal, as both q and k_0 will depend on the pH of the growth experiment. Certainly, the number N of nuclei may change with pH and therefore also q .

As pointed out previously (1), the reaction order m with respect to the aluminate concentration may be evaluated by plotting the function $\log[\alpha(t)^{-2/3} \cdot d\alpha(t)/dt]$ versus $\log(1 - \alpha(t))$ at a fixed temperature and at different pH (pOH) values. Examples of such plots for gibbsite, bayerite and pseudoboehmite the dominant growth phase are given in Fig. 11. For pure gibbsite and bayerite systems these graphs show a straight-line behavior over a wide range of aluminate concentration. When substantial amounts of a second solid phase are indicated during the growth period, deviation from this linear behavior is noted.

It should be noted that similar plots with pseudoboehmite as the growth phase do not yield straight lines. The linear behavior for pseudoboehmite (illustrated in Fig. 11) is obtained when $-\log[1 - \alpha^*(t)]$ instead of $-\log[1 - \alpha(t)]$ is plotted on the x -axis where $\alpha^*(t) = \Delta[\text{H}^+(t)]/(Al_T - Al_E)$ and Al_E , the equilibrium aluminate concentration, is evaluated by assuming pK_{sp} (pseudoboehmite) = -1.1. The growth rate of pseudoboehmite is therefore shown to depend on the concentration difference, $c_{\text{Al}}(t) - c_{\text{Al}}(\text{equil})$.

The exponent n (or the reaction order with respect to the hydrogen ion concentration) may be determined next by plotting $\log k_1$, the intercept on the ordinate axis (Fig. 11), against pH at a fixed temperature. This plot also yields the magnitude of k_2 (see Eq. [26]). Finally on plotting $\ln(k_2 K_{\text{sp}}^m)$ against $1/T$ the activation energy $E_{\text{act}}^{(g)}$ may be evaluated. The absolute value K_{sp} need not be known in this evaluation, only its temperature dependence.

The calculated values of n and m are listed in Table I. Considering the detailed procedure

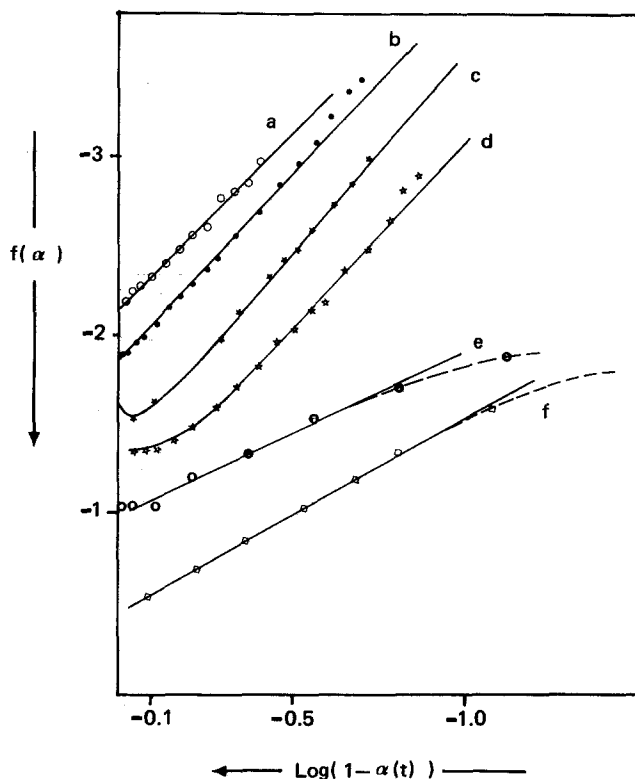


FIG. 11. Illustrative plots of growth rates, $f(\alpha) = \log \times \alpha(t)^{-2/3} \cdot d\alpha/dt$ versus log normalized aluminate concentration, $\log(1 - \alpha(t))$ at different temperatures and different growth phases. (a) Gibbsite: 75°C, pOH 3.35. (b) Bayerite: 50°C, pOH 3.45. (c) Bayerite: 50°C, pOH 3.65. (d) Bayerite: 75°C, pOH 3.85. (e) Pseudoboehmite: 50°C, pOH 4.25. (f) Pseudoboehmite: 75°C, pOH 4.25. On (e) and (f) the x-axis is plotted the function $\log(1 - \alpha^*(t))$, see text.

involved in the evaluation of the activation energy (see Eq. [25]) this growth parameter is known less accurately than the reaction orders. In the temperature range, 50–75°C, where m is roughly equal to n , the activation energy for growth of gibbsite and bayerite is estimated to equal 68 ± 10 kJ/mole. This value corresponds reasonably well with those estimates for gibbsite growth based on seed experiments (17, 21) where also a second-order dependence on supersaturation was observed. Misra and White (17) quote a value of 60 kJ/mole and King (21) 53 kJ/mole for $E_{\text{act}}^{(g)}$.

For bayerite and for gibbsite as growth phase the data of Table I clearly establish a second-order dependence on the aluminate

concentration at all the temperatures investigated. As the nature of the growth unit cannot be directly established from our experiments this second-order dependence may also be interpreted as a first-order dependence on the concentration of a dimer (for example, $\text{Al}_2(\text{OH})_7^-$). Except for measurements at room temperature the reaction order in $[\text{H}^+]$ is seen to be somewhat higher than two. This observation is in general agreement with the assumed dependence of q and probably also k_0 , on pH. A general second-order dependence of the growth of bayerite and gibbsite on the supersaturation Π is therefore not excluded by this investigation.

Once the order m has been established the available surface area A can be determined

from Eq. [21]. The dependence of A on α may be expressed as

$$A(t) = \text{constant } \alpha(t)^z \quad [27]$$

where z may be evaluated by plotting $\log[(1 - \alpha)^{-m} \cdot d\alpha/dt]$ against $\log \alpha$. Note that in Eq. [23] we have assumed $z = 2/3$. In the experiments performed at 50°C only bayerite is the growth phase at low supersaturation (see Fig. 5), the available surface area may then be calculated by taking $m = 2$ and the exponent z by plotting $\log[(1 - \alpha)^{-2}(d\alpha/dt)]$ against $\log \alpha$. This analysis shows that Eq. [27] is a good approximation and yields the values 0.8 (pOH 3.85) and 0.7 (pOH 3.45). Although the calculated range of z values are slightly higher than the value 2/3 (Eq. [23]) this finding may be due to complications, for example, secondary nucleation, introduced during the growth process. Considering, however, the complex nature of the precipitation process and the accuracy attainable by the experimental techniques, we feel justified to conclude that for this system (bayerite growth) the relaxation experiments at different temperatures and pOH values are satisfactorily accounted for by an expression for the growth rate which is proportional to the available surface area and the square of the supersaturation.

As can be seen in Table I there exists a strong correlation between the empirical Π dependence for growth (n) and nucleation (p). We believe it reasonable to expect both the rate of nucleation and of the growth of bayerite to be controlled by the formation of two-dimensional nuclei. This would imply that both rates will be largely determined by the factor $e^{-\Delta G_c(2D)/RT}$ although significant differences may be noted in the preexponential factors.

An analysis of the growth rate of pseudoboehmite by the same procedure used in the analysis of bayerite growth data shows the exponent m to increase strongly with decreasing aluminate concentration. This observation need not be in variance with a

surface nucleation growth mechanism because experiment shows pseudoboehmite to grow at substantially lower supersaturations than bayerite and therefore under conditions where the theory does predict a steep rise in m . Direct proof of the applicability of this mechanism is, however, not available. We have already shown that the experimental growth data for pseudoboehmite fit the empirical relation (see curves e and f, Fig. 11)

$$\dot{R} = k''(T)A(\Pi - 1)^{m'} \quad [28]$$

where, $(\Pi - 1)$ is the relative supersaturation, proportional to the concentration difference, $c_{Al}(t) - c_{Al}(\text{equil})$, and m' is a constant, approximately equal to unity (see Table I). Values for n' describing the dependence of the growth rate on $[H^+]$, are also listed in Table I. The observed functional dependence of \dot{R} on the relative supersaturation $(\Pi - 1)$ instead of the supersaturation, Π (Eq. [21]) is not too surprising because the relatively low supersaturation of the solution with respect to pseudoboehmite combined with the high solubility (pK_{sp} (pseudoboehmite) ≈ -1.1), clearly suggest that the equilibrium concentration, $c_{Al}(\text{equil})$, is not negligible compared to $c_{Al}(t)$. We note, furthermore, that with $m' = 1$, Eq. [28] has the appropriate form for a kinetic process controlled by volume diffusion. A very rough calculation of the growth rates to be expected in our system assuming the kinetics to be diffusion-controlled, yields, however, rates much larger than those observed experimentally. We believe therefore that this interpretation of Eq. [28] may be discarded but are not able to offer a more acceptable alternative. In conclusion we should remark that this empirical relation has also been reported to describe crystal growth rates of a number of simple salts from supersaturated solutions (22).

CONCLUSION

This study confirms the precipitation sequence observed at 25°C (1) in supersaturated

aluminate solution with the appearance of gibbsite at higher temperatures:

amorphous \rightarrow pseudobohemite \rightarrow

bayerite \rightarrow gibbsite.

Regardless of the temperature the least-stable phase is found to precipitate first as predicted by the Ostwald rule of stages. The amorphous phase forms rapidly as is evidenced by the pseudoequilibrium titration curves at fast titration speeds. Its estimated solubility product does not change significantly with temperature; $pK_{sp} \equiv -\log a_{Al(OH)_3}/a_{OH^-} \approx -1.9$. The formation rate of the other phases is measurable and may be interpreted in terms of nucleation and growth mechanisms.

Growth of bayerite is retarded by small amounts of pseudobohemite at all temperatures and from an analysis of the relaxation time curves, a solubility for pseudobohemite ($pK_{sp} \approx -1.3$ to -1.2) which is nearly independent of temperature has been evaluated. Bayerite forms in large amounts at room temperature. At higher temperatures the precipitation rates of pseudobohemite (high pOH values) and gibbsite (at low pOH values) increase faster than that of bayerite (with the result that the latter phase becomes less dominant and may even disappear completely).

Analysis of the experimental relaxation times indicates that the favored formation of pseudobohemite over bayerite at high pOH values is related to its lower interfacial tension and the retarding effect it exerts on bayerite growth. Strong evidence exists that a two-dimensional nucleation mechanism is rate-determining for the formation of bayerite. With this observation as postulate, an analysis of the relaxation time curves in terms of classical nucleation theory allows an estimate of the work of critical nucleation formation ($\Delta G_c \approx 20$ kJ/mole), an overall activation energy for other processes involved ($E_{act}^{(1)} = -30 \pm 10$ kJ/mole) and gives a clear indication that the interfacial tension decreases with increasing temperature. The nu-

cleation of bayerite may also be described by an empirical relation between relaxation time and supersaturation featuring a power law dependence on supersaturation and yields an activation energy $E_{act}^{(2)} \approx 95$ kJ mole $^{-1}$. The difference in the two estimated activation energies may be shown to be largely determined by the standard enthalpy of the precipitation reaction.

The growth rate of bayerite is shown to be proportional to the available surface area and the square of the supersaturation. The activation energy is estimated to have the same magnitude (60–80 kJ/mole) as that observed from gibbsite seed experiments. The growth of pseudobohemite cannot be described by constant power dependence on supersaturation. It is approximately proportional to surface area and the relative supersaturation ($II - 1$).

Finally, we note that the transition from bayerite to gibbsite could not be detected by observable discontinuities or inflections in relaxation times or growth curves. The smooth transition behavior indicates that the formation of these two crystalline phases proceeds by identical mechanisms.

ACKNOWLEDGMENT

The authors wish to thank J. Suurmond for his assistance with the electron-microscopy study of the precipitation products.

REFERENCES

1. Van Straten, H. A., Holtkamp, B. T. W., and de Bruyn, P. L., *J. Colloid Interface Sci.* **98**, 342 (1984).
2. Ostwald, W., *Z. Phys. Chem.* **22**, 289 (1897).
3. Ginsberg, H., Hüttig, W., and Stiehl, H., *Z. Anorg. Allg. Chem.* **309**, 233 (1961).
4. Pohl, K., Meissner, D., and Steinert, W., *Z. Anorg. Allg. Chem.* **343**, 39 (1966).
5. Sato, T., Yamashita, T., and Ozawa, F., *Z. Anorg. Allg. Chem.* **370**, 202 (1969).
6. Stöl, R. J., Doctoral thesis, Utrecht (1978).
7. "Gmelins Handbuch der Anorganische Chemie," p. 1619. Teil Sauerstoff, 8e Auflage, Lieferung, 5.
8. Chang, B.-T., *Bull. Chem. Soc. Jpn.* **54**, 2579 (1981).

9. Russell, A. S., Edwards, J. D., and Taylor, C. D., *Trans. Amer. Inst. Miner. Met. Eng.* **203**, 1123 (1955).
10. Berecz, E., and Szita, C., (ICSOBA, 1969), *Banyasz. Kohasz. Lapok Kohaszat.* **103**, 37 (1970).
11. Chang, B.-T., *Bull. Chem. Soc. Jpn.* **54**, 1960 (1981).
12. Feitknecht, W., and Schindler, P., *Pure Appl. Chem.* **6**, 130 (1963).
13. Dunning, W. J., in "Nucleation" (A. C. Zettlemoyer, Ed.), p. 1. Dekker, New York, 1969.
14. Kuznetsov, S. I., *Tvestn. Met.* **36**, 45 (1963).
15. Glastonbury, J. R., *Chem. Ind.* **6**, 121 (1969).
16. Mal'tsev, G. Z., and Mashovets, V. P., *Zh. Prikl. Khim.* **38**, 92 (1965).
17. Misra, C., and White, E. T., *Chem. Eng. Progr. Symp. Ser.* **67**, 53 (1971).
18. Nielsen, A. E., in "Kinetics of precipitation," p. 18, Pergamon, Oxford, 1964.
19. Bennema, P. J., *Cryst. Growth* **I**, 278 (1967); **24/25**, 76 (1974).
20. Garside, J., in "Crystal Growth and Materials" (E. Kaldis and H. J. Scheel, Eds.), p. 484, North-Holland, Amsterdam, 1977.
21. King, W. R., *Proc. Sess. AIME Ann. Meet. 102nd* **2**, 551 (1973).
22. Nancollas, G. H., *Adv. Colloid Interface Sci.* **10**, 215 (1979).
23. Violante, A., and Violante, P., *Agrochimica* **XXII**, 335 (1978).